Available online at www.sciencedirect.com
SCIENCE DIRECT®
Biochemical and Biophysical Research Communications 336 (2005) 134–141
BBRC
www.elsevier.com/locate/ybbrc

The α_{1S} N-terminus is not essential for bi-directional coupling with RyR1

R.A. Bannister, K.G. Beam *

Department of Biomedical Sciences, Neurosciences Division, Colorado State University, Fort Collins, CO 80523, USA

Received 29 July 2005
Available online 18 August 2005

Abstract

The dihydropyridine receptor (DHPR) α_{1S} II–III loop has been shown to be critical for excitation–contraction (EC) coupling in skeletal muscle, but the importance of other cytoplasmic regions, especially the N-terminus (residues 1–51), remains unclear. In this study, we found that deletion of α_{1S} residues 2–37 (weakly conserved with N-termini of other L-type Ca^{2+} channels) had little effect on the ability of α_{1S} to serve as a Ca^{2+} channel or voltage sensor for EC coupling. Strikingly, deletion of 10 additional residues, which are conserved in L-type channels, resulted in ablation of DHPR function. Specifically, confocal microscopy and measurement of charge movement showed that removal of residues 2–47 resulted in a failure of sarcolemmal insertion. Our results indicate that the weakly conserved, distal α_{1S} N-terminus is not critical for EC coupling or function as a Ca^{2+} channel. However, integrity of the proximal α_{1S} N-terminus is necessary for sarcolemmal expression of the DHPR.

Keywords: Excitation–contraction coupling; DHPR; α_{1S}; $Ca_V1.1$; Skeletal muscle

Voltage-gated Ca^{2+} channels are heteromultimeric complexes containing a primary α_1-subunit and auxiliary $\alpha_2\delta$, β and, in some cases, γ-subunits [1]. The Ca^{2+} channel α_1-subunit forms the Ca^{2+}-conducting pore and houses the voltage-sensing mechanism. Each α_1-subunit is composed of four conserved transmembrane repeats (I–IV), each consisting of six putative α-helices. These repeats are linked by three relatively non-conserved cytoplasmic loops (I–II, II–III, and III–IV), which are important sites for intracellular protein–protein interactions [2–9]. Likewise, the cytoplasmic N- and C-termini of voltage-gated Ca^{2+} channels are also known to interact with signaling and scaffolding molecules [10–19].

The skeletal muscle L-type Ca^{2+} channel (α_{1S}), or dihydropyridine receptor (DHPR), serves as the voltage sensor for excitation–contraction (EC) coupling with the type 1 ryanodine receptor (RyR1), [20]. "Orthograde" coupling between the DHPR and RyR1 is observed as depolarization-induced Ca^{2+} release, which is dependent on channel activation rather than L-type Ca^{2+} current [21–24]. In addition to the orthograde signal, "retrograde" coupling also occurs between the DHPR and RyR1. In *dyspedic* (RyR1 null) myotubes, L-type current density is significantly reduced compared to that of normal myotubes, despite similar DHPR membrane expression [25]. This observation, along with the ability of exogenously expressed RyR1 to restore current density [25–27], supports the conclusion that functional coupling between the DHPR and RyR1 is bi-directional.

A crucial role for the cytoplasmic α_{1S} II–III loop in skeletal-type EC coupling was revealed in experiments that employed a chimeric DHPR consisting of the α_{1S} II–III loop in a cardiac α_{1C}-subunit background [2]. Within the α_{1S} II–III loop, subsequent experiments identified a "critical domain" composed of residues 720–765

* Corresponding author: Fax: +1 970 491 7907.
E-mail address: kbeam@lamar.colostate.edu (K.G. Beam).

0006-291X/$ - see front matter © 2005 Elsevier Inc. All rights reserved.
doi:10.1016/j.bbrc.2005.08.047

[28]. Neither orthograde nor retrograde coupling was supported by a chimera in which the cardiac α_{1C} II–III loop is substituted for the corresponding region of α_{1S}, yet orthograde and retrograde coupling were both rescued by re-introduction of α_{1S} residues 720–764 into the cardiac α_{1C} II–III loop of this construct [29]. A more recent study has proposed that α_{1S} residues 734–748 adopt a random-coil conformation that enables the α_{1S} to interact with other EC coupling proteins [30].

Several lines of evidence suggest that regions in addition to the critical domain of the α_{1S} II–III loop are involved in EC coupling. For example, an α_{1S} mutant, which lacks both the critical domain and an upstream segment of the α_{1S} II–III loop, supports weak EC coupling associated with Ca^{2+} transients about 15% the amplitude of those for wild-type α_{1S} [31]. Additionally, a chimera consisting of α_{1H} with the II–III loop replaced by that of α_{1S} fails to produce skeletal type EC coupling [32] and α_{1S} cytoplasmic domains in addition to the α_{1S} II–III loop affect the voltage dependence of intracellular Ca^{2+} release [33]. Moreover, a variety of experimental approaches suggest that in addition to the α_{1S} II–III loop, the α_{1S} I–II loop [3], α_{1S} III–IV loop [34–36], and α_{1S} C-terminus [17,37,38], as well as the N- and C-termini of β_{1a} [39–42], may be involved in expression and targeting of the DHPR and in its transmission of the EC coupling signal to RyR1. In the case of the α_{1S} N-terminus, it has been found that its replacement by the α_{1C} N-terminus did not affect EC coupling [2,33]. However, the ability of such chimeras to test a role of the α_{1S} N-terminus in EC coupling is limited by structural similarities between α_{1S} and α_{1C} in this region.

In the present study, we examined the effects of deleting portions of the α_{1S} N-terminus, in order to test unambiguously the necessity of this region for EC coupling. Our results indicate that the weakly conserved, distal α_{1S} N-terminus (residues 2–37) is unimportant for bi-directional coupling with RyR1. Deletion of an additional 10 residues, which are completely conserved amongst L-type Ca^{2+} channels (all told, removal of α_{1S} residues 2–47), results in total loss of sarcolemmal expression of the DHPR.

Materials and methods

Molecular biology

α_{1S}-YFP. This construct [42] encodes residues 1–1667 of rabbit α_{1S} [GenBank Accession No. X05921], followed by a 12 residue linker, followed by YFP (239 residues).

$\alpha_{1S}\Delta37$. This construct encodes α_{1S}-YFP with α_{1S} residues 2–37 deleted. Forward primer 5′-cgcgcgcgctagcgccaccatgaacccgctgag gaaggcgt-3′, reverse primer 5′-cgcgcgcgaattccccactcaggacgccc-3′ and PCR (with elongase) were used to produce a cDNA with atg attached to nucleotides 756–1655 of α_{1S}-YFP. The forward primer contained an *Nhe*I restriction enzyme site and the reverse primer an *Eco*RI restriction site that corresponded to an endogenous site at α_{1S}-YFP bp 1650. The resultant PCR product was inserted into α_{1S}-YFP cut with *Nhe*I and *Eco*RI.

$\alpha_{1S}\Delta47$. This construct encodes α_{1S}-YFP minus residues α_{1S} 2–47. Forward primer 5′-gctagcatggtggaatggaaacc-3′ and reverse primer 5′-gaattccccactcaggacgcc-3′ and PCR (with TAQ) were used to attach atg to nucleotides 786–1655 of α_{1S}-YFP. This amplified cDNA was inserted into the TA cloning site of the pCR2.1 cloning vector (Invitrogen, Carlsbad, CA). Subsequently, the pCR2.1 vector containing the inserted cDNA was thoroughly digested with *Eco*RI (cut sites in the polylinker flanking either side of the TA site and at the 3′ end of the inserted cDNA) and the ~900 bp fragment was isolated and ligated into α_{1S}-YFP cut with *Eco*RI. The integrity of each cDNA construct was confirmed by restriction digests and sequencing.

Expression of cDNA

Primary cultures of *dysgenic* myotubes were prepared from newborn mice as described previously [43]. Myoblasts were plated into 35 mm ECL-coated, plastic culture dishes (#353801, Falcon, San Jose, CA) for electrophysiology or onto culture dishes with ECL-coated glass coverslip bottoms (MatTek, Ashland, MA) for confocal microscopy. Cultures were grown for 6–7 days in a humidified 37 °C incubator with 5% CO_2 in Dulbecco's modified Eagle's medium (DMEM; #15-017-CM, Mediatech, Herndon, VA), supplemented with 10% fetal bovine serum/10% horse serum (Hyclone Laboratories, Logan, UT). This medium was then replaced with differentiation medium (DMEM supplemented with 2% horse serum). After 2–4 days, single nuclei were microinjected with 100 ng/μl (for electrophysiology) or 60 ng/μl (for confocal microscopy) cDNA. Expressing myotubes were examined two days after cDNA expression.

Measurement of ionic currents

Pipettes were fabricated from borosilicate glass and had resistances of 2.0–3.0 MΩ when filled with internal solution containing (mM): 140 Cs–aspartate, 10 Cs_2–EGTA, 5 $MgCl_2$, and 10 Hepes, pH 7.4, with CsOH. The external solution contained (mM): 145 TEA-Cl, 10 $CaCl_2$, 0.003 tetrodotoxin (TTX), and 10 Hepes, pH 7.4, with tetraethylammonium (TEA)-OH. Linear capacitative and leakage currents were determined by averaging the currents elicited by eleven, 30 mV hyperpolarizing pulses from a holding potential of −80 mV. Test currents were corrected for linear components of leak and capacitive current by digital scaling and subtraction of this average control current. Electronic compensation was used to reduce the effective series resistance (usually to <1 MΩ) and the time constant for charging the linear cell capacitance (usually to <0.5 ms). Ionic currents were filtered at 2 kHz and digitized at 10 kHz. To measure macroscopic L-type current in isolation, a 1-s prepulse to −20 mV followed by a 100-ms repolarization to −50 mV was administered before the test pulse (prepulse protocol) to inactivate T-type Ca^{2+} channels. Cell capacitance was determined by integration of the current transient evoked from −80 to −70 mV using Clampex 8.0 (Axon Instrument, Foster City, CA). Current–voltage (*I–V*) curves were fitted using the equation:

$$I = G_{max} * (V - V_{rev})/\{1 + \exp[(V_G - V)/k_G]\}, \quad (1)$$

where I is the current for test potential V, V_{rev} is the reversal potential, G_{max} is the maximum Ca^{2+} channel conductance, V_G is the half-maximal activation potential, and k_G is the slope factor.

Measurement of intracellular Ca^{2+} transients

Changes in intracellular Ca^{2+} were recorded with Fluo-3 (Molecular Probes, Eugene, OR). The salt form of the dye was added to the standard internal solution for a final concentration of 200 nM. After entry into the whole-cell configuration, a waiting period of >5 min was used to allow the dye to diffuse into the cell interior. A 100-W mercury

illuminator and a set of fluorescein filters were used to excite the dye present in a small rectangular region of the voltage-clamped myotube. A computer-controlled shutter was used to block illumination in the intervals between test pulses. Fluorescence emission was measured by means of a fluorometer apparatus (Biomedical Instrumentation Group, University of Pennsylvania, Philadelphia, PA). The average background fluorescence was quantified before bath immersion of the patch pipette. Data are expressed as $(\Delta F/F)$, where ΔF represents the change in fluorescence from baseline 50 ms after the onset of the test pulse and F is the fluorescence immediately prior to the test pulse minus the average background (non-Fluo-3) fluorescence. The peak value of the fluorescence change $(\Delta F/F)$ for each test potential (V) was fitted according to

$$(\Delta F/F) = (\Delta F/F)_{max}/\{1 + \exp[(V_F - V)/k_F]\}, \quad (2)$$

where $(\Delta F/F)_{max}$ is the maximal fluorescence change, V_F is the potential causing half the maximal change in fluorescence, and k_F is a slope parameter.

Measurement of charge movements

For measurement of intramembrane charge movements, ionic currents were blocked by the addition of 0.5 mM $CdCl_2$ + 0.1 mM $LaCl_3$ to the extracellular solution. All charge movements were measured with the prepulse protocol (see above) and corrected for linear cell capacitance and leakage currents using a-P/8 subtraction protocol. Filtering was carried out at 2 kHz (eight pole Bessel filter; Frequency Devices) and digitization was at 20 kHz. Voltage clamp command pulses were exponentially rounded with a time constant of 50–500 μs. The integral of the ON transient (Q_{on}) for each test potential (V) was fitted according to

$$Q_{on} = Q_{max}/\{1 + \exp[(V_Q - V)/k_Q]\}, \quad (3)$$

where Q_{max} is the maximal Q_{on}, V_Q is the potential causing movement of half the maximal charge, and k_Q is a slope parameter.

Electrically evoked contractions

Contractions were elicited by 20-ms, 100 V stimuli applied via an extracellular pipette which contained 150 mM NaCl and was placed near intact myotubes expressing constructs of interest. The myotubes were bathed in rodent Ringer's solution (in mM: 146 NaCl, 5 KCl, 2 $CaCl_2$, 1 $MgCl_2$, 10 Hepes, and 11 glucose, pH 7.4, with NaOH). Contractions were assayed by the movement of an identifiable portion of a myotube across the visual field.

Confocal microscopy

Myotubes in rodent Ringer's solution were examined at room temperature using the confocal laser scanning microscope LSM 510 META (Zeiss, Thornwood, NY). An area of 500–2500 μm^2 was selected from the field of view (63× oil immersion objective, 1.4 NA), which included the myotube and also an adjacent, non-cellular region for measurement of background fluorescence. YFP was excited with the 488-nm line of an argon laser (30-mW maximum output, operated at 50% or 6.3 A). The emitted fluorescence was directed to a photomultiplier equipped with a 505-nm long-pass filter. Confocal fluorescence intensity data were recorded as the average of four line scans per pixel and digitized at 8-bits, with photomultiplier gain adjusted such that maximum pixel intensities were no more than ~70% saturated.

Analysis

G_{max}/Q' ratios were only calculated in myotubes where both L-type current and intramembrane charge movements were measured. The average total G_{max} was calculated by Eq. (1) whereas the Q' was derived by subtracting the endogenous charge movement of *dysgenic* myotubes (Q_{dys}) from the average total Q_{max}, where $Q_{dys} = 0.95$ nC/μF (measured at +40 mV). Alignments were made with MacVector (version 7.2.2). All data are presented as means ± SEM. Statistical comparisons were by *ANOVA* or by unpaired, two-tailed t test (as appropriate), with $p < 0.05$ considered significant.

Results

Previous studies to identify regions of α_{1S} of potential importance for EC coupling employed the strategy of constructing chimeric proteins between α_{1S} and α_{1C} [2,28,33] or α_{1A} [44]. This approach can fail to identify regions of functional importance if the regions are sufficiently conserved between the parental proteins. Fig. 1A shows alignments of the primary protein sequences of rabbit α_{1S} [45], rabbit α_{1C} [46], human α_{1D} [47], and rabbit α_{1A} [48]. The protein sequence is identical/conserved between α_{1S}, α_{1C}, and α_{1D} from α_{1S} residue 38 into Repeat I (which begins at α_{1S} residue 52). However, the N-terminus is considerably shorter in α_{1S} than α_{1C} or α_{1D} and is less conserved amongst L-type channels before α_{1S} residue 38 (Fig. 1A). For this reason, we prepared a cDNA that encoded an α_{1S}-subunit that lacked residues 2–37 ($\alpha_{1S}\Delta 37$) to determine whether the less-conserved α_{1S} distal N-terminus may play a specialized role in skeletal-type EC coupling ($\alpha_{1S}\Delta 37$; Fig. 1B, middle). $\alpha_{1S}\Delta 37$ was derived (see Materials and methods) from a parent α_{1S}-YFP fusion construct (hereafter referred to as α_{1S}-YFP; Fig. 1B, top) in which the full-length channel was truncated prior to an endogenous proteolytic cleavage site [49]. Such truncated α_{1S} constructs do not show any obvious functional differences from full-length α_{1S} [42,50].

Deletion of α_{1S} residues 2–37 does not affect DHPR function

Both α_{1S}-YFP and $\alpha_{1S}\Delta 37$ produced large-amplitude L-type Ca^{2+} currents (bottom panels, Figs. 2A and B, respectively) that were much like those previously reported for full-length GFP-α_{1S} constructs [51–53]. Furthermore, the Ca^{2+} currents for $\alpha_{1S}\Delta 37$ had a voltage-dependence similar to that of the Ca^{2+} currents for α_{1S}-YFP (Fig. 2C, Table 1). Also having similar voltage-dependence were the charge movements produced by the two constructs (Fig. 2D, Table 1). It should be noted that there was a statistically significant ($p < 0.022$) reduction in the peak current density for $\alpha_{1S}\Delta 37$ (-3.9 ± 0.3 pA/pF at +40 mV; $n = 16$) compared to α_{1S}-YFP (-5.1 ± 0.3 pA/pF; $n = 37$). This reduction in peak current density was probably a consequence of reduced DHPR expression since maximal charge movements were also reduced ($Q_{max} = 5.0 \pm 0.5$ nC/μF, $n = 5$ vs 6.0 ± 0.4 nC/μF; $n = 8$, respectively, for $\alpha_{1S}\Delta 37$ and α_{1S}-YFP). Consequently, in the subset of

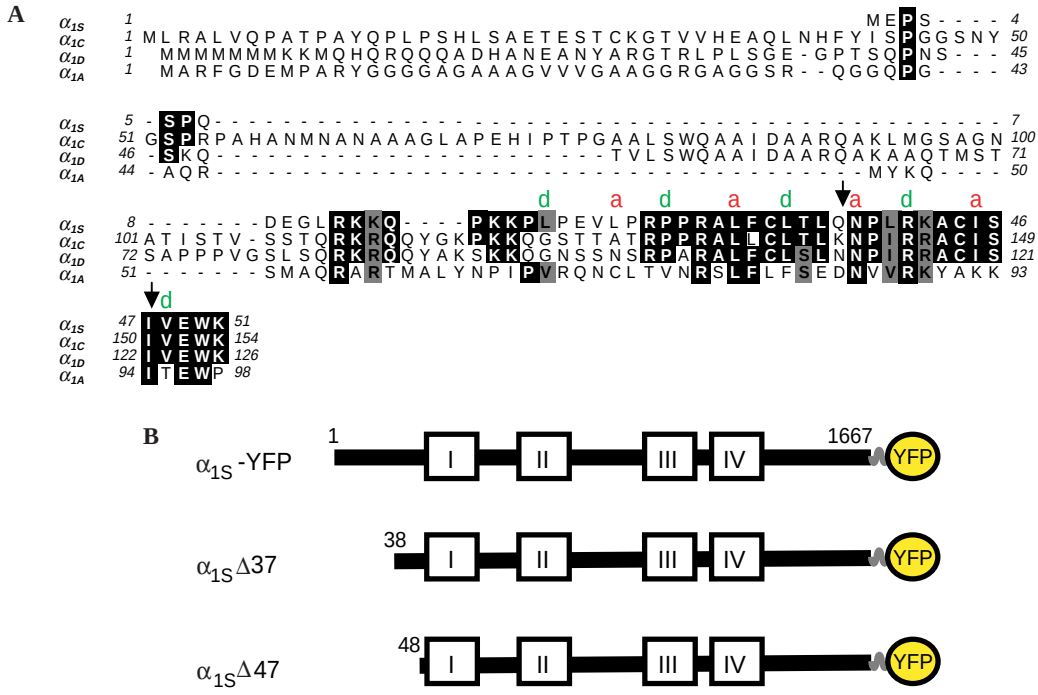

Fig. 1. Sequence comparison of the N-termini of α_{1S}, α_{1C}, α_{1D}, and α_{1A}, and schematic representation of α_{1S} deletion constructs. (A) Sequence comparison of rabbit α_{1S} [GenBank Accession No. X05921], rabbit α_{1C} [GenBank Accession No. X15539], human α_{1D} [GenBank Accession No. NM000721], and rabbit α_{1A} [GenBank Accession No. X57477]. Identical residues are shown in bold and boxed in black. Similar residues are shown in bold and boxed in gray. Red a's and green d's denote residues in the a and d positions, respectively, of the imperfect leucine zipper (LZ)-like motif [54]. Arrows indicate the position of deletions depicted in (B). (B) Schematic representation of the α_{1S} constructs: top, α_{1S}; YFP middle, $\alpha_{1S}\Delta37$; bottom, $\alpha_{1S}\Delta47$. Numbers refer to amino acid residues of α_{1S}. Wavy lines represent a 12-residue linker between α_{1S} and YFP (see Materials and methods for construction details). (For interpretation of the references to colors in this figure legend, the reader is referred to the web version of this paper.)

experiments where both L-type currents and charge movements were obtained, the G_{max}/Q' ratio (see Materials and methods for calculation) was virtually identical for myotubes expressing α_{1S}-YFP and $\alpha_{1S}\Delta37$ (32.6 vs 34.8, respectively). Thus, the reduced current density was likely a consequence of decreased membrane expression, rather than reduced retrograde coupling with RyR1 (Table 1). This decreased membrane expression has a number of possible explanations, but its small size suggests that the weakly conserved, distal α_{1S} N-terminus has little or no role in regulating the biosynthesis or membrane targeting of the DHPR.

Myoplasmic Ca^{2+} transients were measured to assess potential effects of deletion of α_{1S} residues 2–37 on orthograde coupling. α_{1S}-YFP and $\alpha_{1S}\Delta37$ both triggered robust Ca^{2+} transients (top panels, Figs. 2A and B, respectively) that had a similar sigmoidal dependence on test potential (Fig. 2E, Table 1), a hallmark of skeletal-type EC coupling [24]. In addition to having similar voltage-dependence, Ca^{2+} transients for α_{1S}-YFP and $\alpha_{1S}\Delta37$ also had similar amplitudes: $(\Delta F/F)_{max}$ of 0.58 ± 0.09 ($n = 15$) and 0.51 ± 0.14 ($n = 6$), respectively (not significantly different, $p > 0.67$). Likewise, electrically evoked contractions were observed for both $\alpha_{1S}\Delta37$ (23 of 41 myotubes tested) and YFP-α_{1S} (41 of 47 myotubes tested). Altogether, these data indicate that the amino acids 2–37 of α_{1S} are not directly involved in orthograde coupling between RyR1 and the DHPR.

Deletion of α_{1S} residues 2–47 ablates DHPR membrane expression

To determine whether highly conserved residues in the α_{1S} N-terminus (specifically, α_{1S} residues 38–47) may be important for EC coupling, we prepared a cDNA that encoded an α_{1S}- subunit lacking residues 2–47 ($\alpha_{1S}\Delta47$; Fig. 1B, bottom). Deletion of the N-terminal 47 residues of α_{1S} left 5 residues (including the start methionine) prior to the first putative membrane-embedded α-helix of repeat I (Fig. 1A), [45]. In contrast to myotubes expressing $\alpha_{1S}\Delta37$ (Fig. 2), myotubes expressing $\alpha_{1S}\Delta47$ lacked significant L-type current (Fig. 3A; $n = 15$) and thus resembled uninjected *dysgenic* myotubes ($n = 7$; Fig. 3A). The ability of $\alpha_{1S}\Delta47$ to support myoplasmic Ca^{2+} release was not examined because of: (1) the lack of evoked contractions in myotubes expressing $\alpha_{1S}\Delta47$ ($n = 22$); and (2) the apparent lack of DHPR membrane expression (see below).

When viewed with confocal microscopy, junctionally targeted, fluorescent protein-tagged skeletal muscle DHPRs are observed as punctate foci on the myotube surface [42,51]. As expected from the ability to support EC

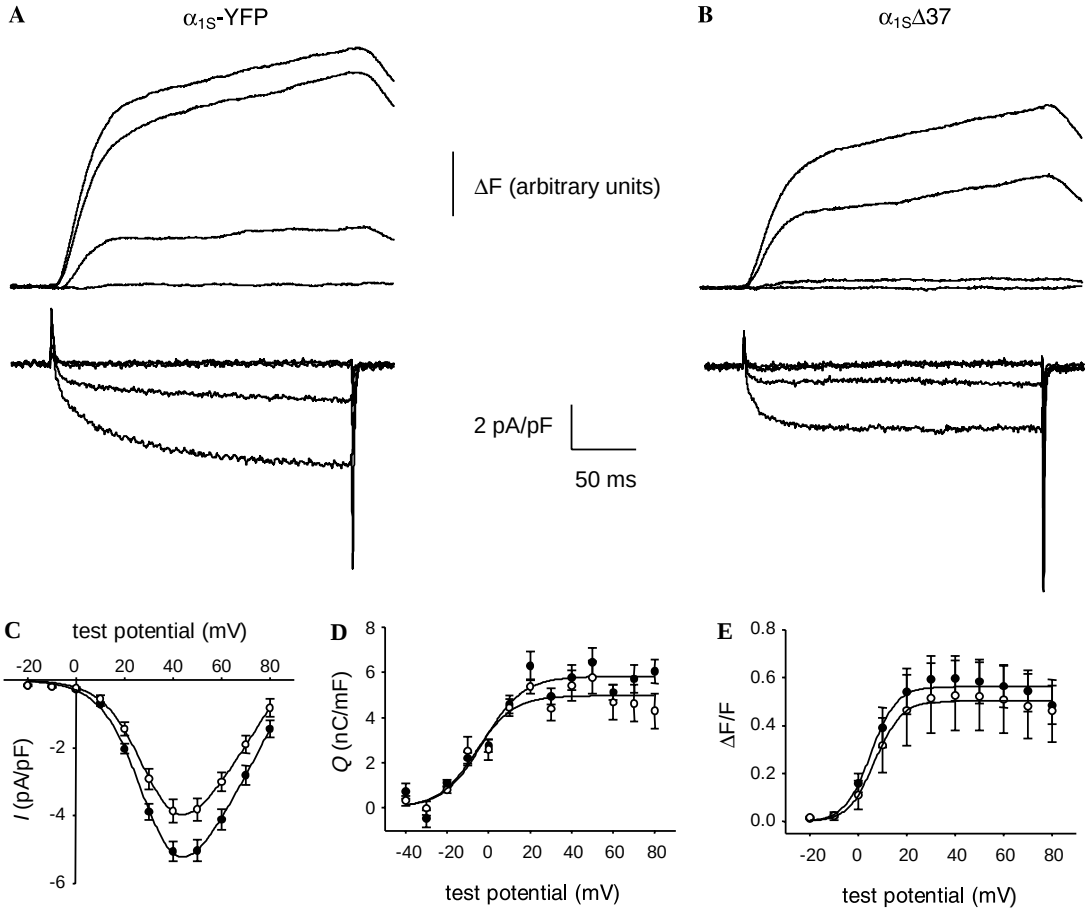

Fig. 2. Deletion of α_{1S} residues 2–37 has little effect on bi-directional coupling. Simultaneous recordings of myoplasmic Ca^{2+} transients (top) and L-type Ca^{2+} currents (bottom), elicited by 200-ms depolarizations to the indicated test potentials, are shown for *dysgenic* myotubes expressing either α_{1S}-YFP (A) or $\alpha_{1S}\Delta37$ (B). (C) *I–V* relationships for α_{1S}-YFP (●; $n = 26$) and $\alpha_{1S}\Delta37$ (○; $n = 16$). (D) *Q–V* relationships for α_{1S}-YFP (●; $n = 8$) and $\alpha_{1S}\Delta37$ (○; $n = 5$). Charge movements were measured with 20 ms depolarizations from −50 mV (See Materials and methods). (E) $\Delta F/F - V$ relationships for α_{1S}-YFP (●; $n = 15$) and $\alpha_{1S}\Delta37$ (○; $n = 6$). Throughout, error bars represent ± SEM. The smooth *I-V* curves are plotted according to Eq. (1). Sigmoidal $\Delta F/F - V$ and *Q–V* curves are plotted according to Eqs. (2) and (3), respectively. The best fit parameters for each plot are presented in Table 1.

Table 1
Ca^{2+} conductance, intramembrane charge movement, and Ca^{2+} transients of α_{1S}-YFP constructs

	G_{max} (nS/nF)	V_G (mV)	k_G (mV)	Q_{max} (nC/μF)	V_Q (mV)	k_Q (mV)	G_{max}/Q'_{max} (nS/pC)	$(\Delta F/F)_{max}$ ($\Delta F/F$)	V_F (mV)	k_F (mV)
α_{1S}-YFP	140 ± 5 (37)	31.2 ± 0.8	8.1 ± 0.2	6.0 ± 0.4 (8)	9.0 ± 0.7	−3.2 ± 2.0	32.6 (8)	0.58 ± 0.09 (15)	4.7 ± 0.4	6.6 ± 1.6
$\alpha_{1S}\Delta37$	119 ± 9 (16)	32.8 ± 1.4	8.8 ± 0.6	5.0 ± 0.5 (5)	9.2 ± 1.5	−5.8 ± 1.6	34.8 (5)	0.51 ± 0.14 (6)	5.1 ± 0.5	8.3 ± 2.3
$\alpha_{1S}\Delta47$	No inward current (15)			NF			ND	ND		
Uninjected *dysgenic* myotubes	No inward current (7)			NF			ND	ND		

Data are given as means ± SEM, with the numbers in parentheses indicating the number of myotubes tested. See Materials and methods for fits. *Q–V* relationships for $\alpha_{1S}\Delta47$ and uninjected *dysgenic* myotubes are labeled "NF" because these data could not be fitted by the appropriate equation. Q'_{max} is the difference between Q_{max} and the endogenous charge movement of *dysgenic* myotubes (0.95 nC/μF; measured at +40 mV). For all the data given, the calculated average voltage error was <5 mV.

coupling, α_{1S}-YFP and $\alpha_{1S}\Delta37$ each localized to punctate foci (Fig. 3B, top and middle), indicating that both constructs were properly targeted to the triad junction. In contrast, no obvious fluorescence puncta were evident in cell myotubes expressing $\alpha_{1S}\Delta47$ and the fluorescence was restricted to the region of the myotube near the injected nucleus, suggesting that the translated protein was unable to traffic to the plasma membrane (Fig. 3B, bottom). Intramembrane charge movement was measured to confirm the absence of membrane expression. The maximal

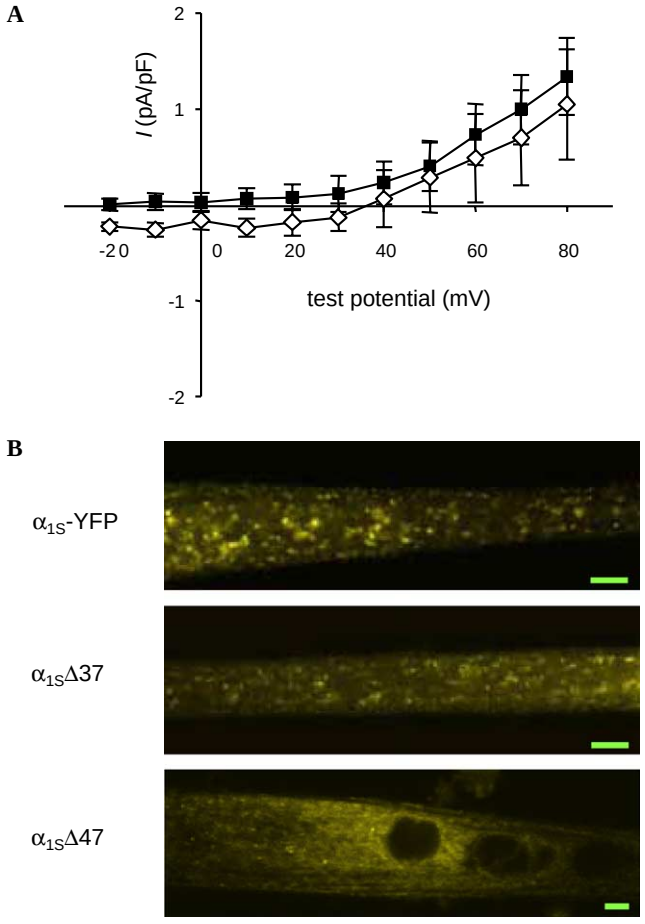

Fig. 3. Deletion of α_{1S} residues 2–47 ablates DHPR membrane expression. (A) unfitted *I–V* relationships for *dysgenic* myotubes expressing $\alpha_{1S}\Delta47$ (■; $n = 12$) and uninjected *dysgenic* myotubes (◇; $n = 7$). (B) Confocal images of yellow fluorescence are shown of *dysgenic* myotubes expressing: α_{1S}-YFP (top), $\alpha_{1S}\Delta37$ (middle), and $\alpha_{1S}\Delta47$ (bottom). *X–Y* scans were made with similar laser settings and show a plane close to the myotube surface. Bar, 5 μm. (For interpretation of the references to colors in this figure legend, the reader is referred to the web version of this paper.)

charge movement (measured at +40 mV) of *dysgenic* myotubes expressing $\alpha_{1S}\Delta47$ (0.84 ± 0.17 nC/μF; $n = 5$) was not different from that of uninjected *dysgenic* myotubes (0.95 ± 0.33 nC/μF; $n = 5$). These results indicate that proximal α_{1S} N-terminus (α_{1S} residues 38–47) is important for either proper folding of the channel protein or export of the channel to the plasma membrane.

Discussion

The two main findings of this study are: (1) removal of the weakly conserved, distal portion of the α_{1S} N-terminus (residues 2–37) has no effect on bi-directional coupling between the DHPR and RyR1; and (2) the additional removal of the proximal, conserved residues 38–47 ablates sarcolemmal expression of the DHPR. In regard to the first of these two findings, earlier studies showed that substitution of the α_{1C} N-terminus for that of α_{1S} does not alter skeletal EC coupling [2,33]. Additionally, junctional targeting of DHPRs was found not to be affected when the α_{1S} N-terminus was replaced by the α_{1A} N-terminus [44]. These results are now greatly strengthened by the demonstration that complete deletion of α_{1S} residues 2–37 has essentially no effect on either Ca^{2+} currents or EC coupling (Fig. 2). Accordingly, these residues must not play an important role in either the function or targeting of DHPRs. The role in signaling of the more proximal residues (38–47), which are conserved/identical amongst L-type Ca^{2+} channels, is less clear because removing them together with residues 2–37 resulted in a loss of membrane expression as judged by the absence both of fluorescent foci near the cell surface (Fig. 3) and of intramembrane charge movement (Table 1). Possibly, these proximal ten residues, which also are 50% conserved in α_{1A} (Fig. 1A), govern trafficking through the biosynthetic pathway, although it is also quite possible that their absence leads to misfolding of the channel protein.

In a past attempt to identify interaction partners for the α_{1S} N-terminus, our laboratory has employed a yeast-2-hybrid screen [Proenza and Beam, unpublished results]. This screen failed to produce any potential interaction partners, but this does not imply that no such interaction partners exist. Examination of the α_{1S} N-terminus reveals the presence of at least two putative protein-protein interaction domains: a PXXP motif (amino acids 3–6) and an imperfect leucine zipper (LZ)-like motif (α_{1S} amino acids 24–47), [54]. PXXP motifs bind to src-homology 3 (SH3) interaction domains [55] which are present in a myriad of proteins, including the MAGUK family of scaffolding proteins. The Ca_V β-subunits contain an SH3 domain, but it is thought to be inactive [7–9] and thus unlikely to represent an interaction partner. In fact, binding of the N-terminal PXXP motif of α_{1S} to any SH3 domain seems unlikely to be critical for basic function of α_{1S} since its deletion had little effect. However, a modulatory role remains a possibility.

LZ motifs are formed by hydrophobic amino acids lining a face of an α-helix and are potential interaction sites for LZ motifs of other proteins [56]. In some cases, leucine residues are substituted by isoleucine, valine or occasionally non-hydrophobic residues to form LZ-like motifs, which are functionally equivalent to true LZ motifs [54]. Perhaps, the complete ablation of DHPR membrane expression with $\alpha_{1S}\Delta47$ (Fig. 3) may have been a consequence of elimination of the entire N-terminal LZ-like motif. In regard to possible interaction partners for the N-terminal LZ-like motif, skeletal and cardiac DHPRs both contain LZ-like domains in their respective C-termini, which have been reported to mediate interactions with the scaffold protein AKAP15 [18,19].

The DHPR β_{1a}-subunit also contains an LZ-like, heptad-repeat domain in the variable D5 region of the C-terminus and disruption of this domain impairs skeletal-type EC coupling [39–41]. Because an α_1–β interaction site in addition to the I–II loop [3] has recently been proposed [57,58], it is tantalizing to speculate that the LZ-like domain of the α_{1S} N-terminus may interact with the heptad repeat of the β_{1a} C-terminus to promote channel expression and subsequently facilitate bi-directional coupling. RyR1 has many LZ domains [54] and therefore a direct interaction between the DHPR N-terminus and RyR1 via a LZ interaction is also an intriguing possibility.

In conclusion, the distal, weakly conserved portion of the α_{1S} N-terminus does not appear to have an important role in the expression of the skeletal DHPR or in the bi-directional interactions of the DHPR with RyR1. The deletion of the more proximal, highly conserved α_{1S} N-terminus led to a loss of membrane expression. It remains an open question as to whether this region is important for bi-directional signaling and an important goal for future experiments will be to determine whether this portion of the N-terminus interacts with other regions of α_{1S}, or with other known (e.g., β_{1a}, RyR1) or unknown junctional proteins.

Acknowledgments

We thank Drs. C.S. Haarmann, V. Leuranguer, N.M. Lorenzon, D.C. Sheridan, and Mr. E.E. Norris for insightful discussion. We thank Ms. A. Krueger and Ms. L. Bederka for their expert technical assistance. This work was supported in part by National Institutes of Health Grants NS24444 and AR44750 (to K.G.B.). R.A.B. was supported by an NIH training Grant NS543115.

References

[1] T.P. Snutch, J. Peloquin, E. Mathews, J.E. McRory, Molecular properties of voltage-gated calcium channels, in: G.W. Zamponi (Ed.), Voltage-gated Calcium Channels, Kluwer Academic/Plenum, New York, 2004, pp. 61–94.

[2] T. Tanabe, K.G. Beam, B.A. Adams, T. Niidome, S. Numa, Regions of the skeletal muscle dihydropyridine receptor critical for excitation–contraction coupling, Nature 346 (1990) 567–569.

[3] M. Pragnell, M. De Waard, Y. Mori, T. Tanabe, T.P. Snutch, K.P. Campbell, Calcium channel beta-subunit binds to a conserved motif in the I–II cytoplasmic linker of the alpha-1 subunit, Nature 368 (1994) 67–70.

[4] Z.-H. Sheng, J. Rettig, M. Takahashi, W.A. Catterall, Identification of a syntaxin-binding site on N-type calcium channels, Neuron 13 (1994) 1303–1313.

[5] M. De Waard, H.Y. Liu, D. Walker, V.E.S. Scott, C.A. Gurnett, K.P. Campbell, Direct binding of G-protein $\beta\gamma$ complex to voltage-dependent calcium channels, Nature 385 (1997) 446–450.

[6] G.W. Zamponi, E. Bourinet, D. Nelson, J. Nargeot, T.P. Snutch, Crosstalk between G-proteins and protein kinase C mediated by the calcium channel α1-subunit, Nature 385 (1997) 442–446.

[7] Y. Chen, M. Li, Y. Zhang, L. He, Y. Yamada, A. Fitzmaurice, Y. Shen, H. Zhang, L. Tong, J. Yang, Structural basis of the α1–β-subunit interaction of voltage-gated Ca^{2+} channels, Nature 429 (2004) 675–680.

[8] Y. Opatowsky, C.-C. Chen, K.P. Campbell, J.A. Hirsch, Structural analysis of the voltage-dependent calcium channel β-subunit functional core and its complex with the α1 interaction domain, Neuron 42 (2004) 387–399.

[9] F. Van Petegem, K.A. Clark, F.C. Chatelain, D.L. Minor, Structure of a complex between a voltage-gated calcium channel β-subunit and an α-subunit domain, Nature 429 (2004) 670–675.

[10] N. Qin, D. Platano, R. Olcese, E. Stefani, L. Birnbaumer, Direct binding of G$\beta\gamma$ with a C-terminal $\beta\gamma$-binding domain of the Ca^{2+} channel α1-subunit is responsible for channel inhibition by G-protein coupled receptors, Proc. Natl. Acad. Sci. USA 94 (1997) 8866–8871.

[11] K.M. Page, C. Cantí, G.J. Stephens, N.S. Berrow, A.C. Dolphin, Identification of the amino terminus of neuronal Ca^{2+} channel α1 subunits of α1B and α1E as an essential determinant of G-protein modulation, J. Neurosci. 18 (1998) 4815–4824.

[12] H.L. Alger, J. Evans, L.H. Tay, M.J. Anderson, H.M. Colecraft, D.T. Yue, G protein-gated inhibitory module of N-type ($Ca_V2.2$) Ca^{2+} channels, Neuron 46 (2005) 891–904.

[13] A. Lee, S.T. Wong, D. Gallagher, B. Li, D.R. Storm, T. Scheuer, W.A. Catterall, Ca^{2+}/calmodulin binds to and modulates P/Q-type calcium channels, Nature 399 (1999) 155–159.

[14] B.Z. Peterson, C.D. DeMaria, D.T. Yue, Calmodulin is the Ca^{2+} sensor for Ca^{2+}-dependent inactivation of L-type channels, Neuron 22 (1999) 549–558.

[15] N. Qin, R. Olcese, M. Bransby, T. Lin, L. Birnbaumer, Ca^{2+}-induced inhibition of the cardiac Ca^{2+} channel depends on calmodulin, Proc. Natl. Acad. Sci. USA 96 (1999) 2435–2438.

[16] R.D. Zühlke, G.S. Pitt, K. Deisseroth, R.W. Tsien, H. Reuter, Calmodulin supports both inactivation and facilitation of L-type calcium channels, Nature 399 (1999) 159–162.

[17] C. Proenza, C.M. Wilkens, N.M. Lorenzon, K.G. Beam, A C-terminal region important for the expression and targeting of the skeletal muscle dihydropyridine receptor, J. Biol. Chem. 275 (2000) 23169–23174.

[18] J.T. Hulme, M. Ahn, S.D. Hauschka, T. Scheuer, W.A. Catterall, A novel leucine zipper targets AKAP15 and cyclic AMP-dependent protein kinase to the C terminus of the skeletal muscle Ca^{2+} channel and modulates its function, J. Biol. Chem. 277 (2002) 4079–4087.

[19] J.T. Hulme, T.W. Lin, R.E. Westenbroek, T. Scheuer, W.A. Catterall, β-Adrenergic regulation requires direct anchoring of PKA to cardiac $Ca_V1.2$ channels via a leucine zipper interaction with A kinase-anchoring protein 15, Proc. Natl. Acad. Sci. USA 100 (2003) 13093–13098.

[20] R.T. Dirksen, Bi-directional coupling between dihydropyridine receptors and ryanodine receptors, Front. Biosci. 7 (2002) d659–d670.

[21] M.F. Schneider, W.K. Chandler, Voltage dependence charge movement in skeletal muscle: a possible step in excitation-contraction coupling, Nature 242 (1973) 244–246.

[22] E. Ríos, G. Brum, Involvement of dihydropyridine receptors in excitation–contraction coupling in skeletal muscle, Nature 325 (1987) 717–720.

[23] T. Tanabe, K.G. Beam, J.A. Powell, S. Numa, Restoration of excitation–contraction coupling and slow calcium current in dysgenic muscle by dihydropyridine receptor complementary DNA, Nature 336 (1988) 134–139.

[24] J. Garcia, K.G. Beam, Measurement of calcium transients and slow calcium current in myotubes, J. Gen. Physiol. 103 (1994) 107–123.

[25] J. Nakai, R.T. Dirksen, H.T. Nguyen, I.N. Pessah, K.G. Beam, P.D. Allen, Enhanced dihydropyridine receptor channel activity in the presence of ryanodine receptor, Nature 380 (1996) 72–75.
[26] J. Nakai, N. Sekiguchi, T.A. Rando, P.D. Allen, K.G. Beam, Two regions of the ryanodine receptor involved in coupling with L-type Ca^{2+} channels, J. Biol. Chem. 273 (1998) 13403–13406.
[27] G. Avila, R.T. Dirksen, Functional impact of the ryanodine receptor on the skeletal muscle L-type Ca^{2+} channel, J. Gen. Physiol. 115 (2000) 467–480.
[28] J. Nakai, T. Tanabe, T. Konno, B.A. Adams, K.G. Beam, Localization in the II–III loop of the dihydropyridine receptor of a sequence critical for excitation–contraction coupling, J. Biol. Chem. 273 (1999) 24983–24986.
[29] M. Grabner, R.T. Dirksen, N. Suda, K.G. Beam, The II–III loop of the skeletal muscle dihydropyridine receptor is responsible for the bi-directional coupling with the ryanodine receptor, J. Biol. Chem. 274 (1999) 21913–21919.
[30] G. Kugler, R.G. Weiss, B.E. Flucher, M. Grabner, Structural requirements of the dihydropyridine receptor α1S II–III loop for skeletal-type excitation–contraction coupling, J. Biol. Chem. 279 (2004) 4721–4728.
[31] C.A. Ahern, D. Bhattacharya, L. Mortensen, R. Coronado, A component of excitation–contraction coupling triggered in the absence of the T671–Q765 regions of the II–III loop of the dihydropyridine receptor α1S pore subunit, Biophys. J. 81 (2001) 3294–3307.
[32] C.M. Wilkens, K.G. Beam, Insertion of α1S II–III loop and C terminal sequences into α1H fails to restore excitation-contraction coupling in dysgenic myotubes, J. Musc. Res. Cell Mot. 24 (2003) 99–109.
[33] L. Carbonneau, D. Bhattacharya, D.C. Sheridan, R. Coronado, Multiple loops of the dihydropyridine receptor pore subunit are required for full-scale excitation–contraction coupling in skeletal muscle, Biophys. J. 89 (2005) 243–255.
[34] P. Leong, D.H. MacLennan, A 37-amino acid sequence in the skeletal muscle ryanodine receptor interacts with the cytoplasmic loop between domains II and III in the skeletal muscle dihydropyridine receptor, J. Biol. Chem. 273 (1998) 7791–7794.
[35] P. Leong, D.H. MacLennan, The cytoplasmic loops between domains II and III and domains III and IV in the skeletal muscle dihydropyridine receptor bind to contiguous site in the skeletal muscle ryanodine receptor, J. Biol. Chem. 273 (1998) 29958–29964.
[36] R.G. Weiss, K.M.S. O'Connell, B.E. Flucher, P.D. Allen, M. Grabner, R.T. Dirksen, Functional analysis of the R1086H malignant hyperthermia mutation in the DHPR reveals an unexpected influence of the III–IV loop on skeletal muscle EC coupling, Am. J. Physiol. 287 (2004) C1094–C1102.
[37] S. Sencer, R.V. Papineni, D.B. Halling, P. Pate, J. Krol, J.Z. Zhang, S.L. Hamilton, Coupling of RYR1 and L-type calcium channels via calmodulin binding domains, J. Biol. Chem. 276 (2001) 38237–38241.
[38] N.M. Lorenzon, C.S. Haarmann, E.E. Norris, S. Papadopoulos, K.G. Beam, Metabolic biotinylation as a probe of supramolecular structure of the triad junction in skeletal muscle, J. Biol. Chem. 279 (2004) 44057–44064.
[39] M. Beurg, C.A. Ahern, P. Vallejo, M.W. Conklin, P.A. Powers, R.G. Gregg, R. Coronado, Involvement of the carboxy-terminus region of the dihydropyridine receptor β_{1a} subunit in excitation–contraction coupling of skeletal muscle, Biophys. J. 77 (1999) 2953–2967.
[40] D.C. Sheridan, W. Cheng, C.A. Ahern, L. Mortensen, D. Alsammarae, P. Vallejo, R. Coronado, Truncation of the carboxyl terminus of the dihydropyridine receptor β1a subunit promotes Ca^{2+} dependent excitation–contraction coupling in skeletal myotubes, Biophys. J. 84 (2003) 220–237.
[41] D.C. Sheridan, W. Cheng, L. Carbonneau, C.A. Ahern, R. Coronado, Involvement of a heptad repeat in the carboxyl terminus of the dihydropyridine receptor β1a subunit in the mechanism of excitation–contraction coupling in skeletal muscle, Biophys. J. 87 (2004) 929–942.
[42] S. Papadopoulos, V. Leuranguer, R.A. Bannister, K.G. Beam, Mapping sites of potential proximity between the DHPR and RyR1 in muscle using a CFP-YFP tandem as a FRET probe, J. Biol. Chem. 279 (2004) 44046–44056.
[43] K.G. Beam, C. Franzini-Armstrong, Functional and structural approaches to the study of excitation–contraction coupling, Methods Cell. Biol. 52 (1997) 283–306.
[44] B.E. Flucher, N. Kasielke, M. Grabner, The triad targeting signal of the skeletal muscle calcium channel is localized in the COOH terminus of the α_{1S}-subunit, J. Cell Biol. 151 (2000) 467–478.
[45] T. Tanabe, H. Takeshima, A. Mikami, V. Flockerzi, H. Takahashi, K. Kangawa, M. Kojima, H. Matsuo, T. Hirose, S. Numa, Primary structure of the receptor for calcium channel blockers from skeletal muscle, Nature 328 (1987) 313–318.
[46] A. Mikami, K. Imoto, T. Tanabe, T. Niidome, Y. Mori, H. Takeshima, S. Narumiya, S. Numa, Primary structure and functional expression of the cardiac dihydropyridine-sensitive calcium channel, Nature 86 (1989) 85–89.
[47] M.E. Williams, D.H. Feldman, A.F. McCue, R. Brenner, G. Velicelebi, S.B. Ellis, M.M. Harpold, Structure and functional expression of alpha1, alpha2, and beta subunits of a novel human neuronal calcium channel subtype, Neuron 8 (1992) 71–84.
[48] Y. Mori, T. Friedrich, M.S. Kim, A. Mikami, J. Nakai, P. Ruth, E. Bosse, F. Hofmann, V. Flockerzi, T. Furuichi, K. Mikoshiba, K. Imoto, T. Tanabe, S. Numa, Primary structure and functional expression from complementary cDNA of a brain calcium channel, Nature 350 (1991) 398–402.
[49] K.S. De Jongh, D.K. Merrrick, W.A. Catterall, Subunits of purified calcium channels: a 212-kDa form of α1 and partial amino acid sequence of a phosphorylation site of an independent β-subunit, Proc. Natl. Acad. Sci. USA 86 (1989) 8585–8589.
[50] K.G. Beam, B.A. Adams, T. Niidome, S. Numa, T. Tanabe, Function of a truncated dihydropyridine receptor as both voltage sensor and calcium channel, Nature 360 (1992) 169–171.
[51] M. Grabner, R.T. Dirksen, K.G. Beam, Tagging with green fluorescent protein reveals a distinct subcellular distribution of L-type and non-L-type Ca^{2+} channels expressed in dysgenic myotubes, Proc. Natl. Acad. Sci. USA 95 (1998) 1903–1908.
[52] C.M. Wilkens, N. Kasielke, B.E. Flucher, K.G. Beam, M. Grabner, Excitation–contraction coupling is unaffected by drastic alteration of the sequence surrounding residues L720–L764 of the alpha1S II–III loop, Proc. Natl. Acad. Sci. USA 98 (2001) 5892–5897.
[53] B.E. Flucher, R.G. Weiss, M. Grabner, Cooperation of two-domain Ca^{2+} channel fragments in triad targeting and restoration of excitation–contraction coupling in skeletal muscle, Proc. Natl. Acad. Sci. USA 99 (2002) 10167–10172.
[54] S.O. Marx, S. Reiken, Y. Hisamatsu, M. Gaburjakova, J. Gaburjakova, Y.-M. Yang, N. Rosemblit, A.R. Marks, Phosphorylation-dependent regulation of ryanodine receptors: a novel role for leucine/isoleucine zippers, J. Cell Biol. 153 (2001) 699–708.
[55] T. Pawson, P. Nash, Assembly of cell regulatory systems through protein interaction domains, Science 300 (2003) 445–452.
[56] S.N. MacFarlane, I.B. Levitan, Unzipping ion channels, Science STKE 2001 (2001) 1–2.
[57] S.X. Takahashi, J. Miriyala, H.M. Colecraft, Membrane-associated guanylate kinase-like properties required for modulation of voltage-dependent Ca^{2+} channels, Proc. Natl. Acad. Sci. USA 101 (2004) 193–198.
[58] S.X. Takahashi, S. Dalton, J. Miriyala, H.M. Colecraft, Differential regulation of Ca^{2+} channel trafficking and gating by molecular distance between β-subunit SH3/GK domains, Biophys. J. 88 (2005) 200a.